Materials Science-Poland, 38(4), 2020, pp. 699-706
http://www.materialsscience.pwr.wroc.pl/
DOI: 10.2478/msp-2020-0073

sciendo

Structural-phase transformations in 0.34C–1CRr–1Ni–1Mo–Fe steel during plasma electrolytic hardening

B.K. RAKHADILOV[1], R.S. KOZHANOVA[2,*], N.A. POPOVA[3], A.B. NUGUMANOVA[1], A.B. KASSYMOV[4]

[1]Non-profit limited company Sarsen Amanzholov East Kazakhstan University, 30 Gvardeiskoi Divisii St. 34, 070020, Kazakhstan

[2]Plasma Science LLP, 37 Serikbaev St., 070010, Kazakhstan

[3]Tomsk State Architecture and Building University, 2 Solyanaya Sq., 634003, Russia

[4]Shakarim University, 20A Glinka St., 071412, Kazakhstan

Structural-phase transformations in 0.34C–1Cr–1Ni–1Mo–Fe steel during plasma electrolytic hardening were investigated. Electrolytic-plasma hardening of steel samples was carried out by surface quenching with rapid concentrated heating of the surface by plasma action and subsequent rapid cooling by heat removal from the depth of the sample by electrolyte jet. Plasma electrolytic hardening was carried out in the cathode mode in an electrolyte made from an aqueous solution containing 20 % sodium carbonate and 10 % carbamide. To study the structural-phase states of the modified layer, we used the method of transmission diffraction electron microscopy on thin foils. The study of steel samples was carried out before and after the plasma electrolytic hardening. Initially, the steel was a mixture of pearlite and ferrite grains. Surface hardening of 0.34C–1Cr–1Ni–1Mo–Fe ferrite-pearlite steel led to a change in the structural-phase state and the formation of a packet-lamellar martensite structure. It was found that PEH leads to distortion of the crystal lattice and the formation of long-range internal stresses, as well as to the release of small particles of cementite and carbide of M23C6 type, uniformly distributed throughout the volume of the material. Surface hardening led to the increase in all quantitative parameters of the fine structure (ρ, ρ ±, χ, σL, σd).

Keywords: *electrolyte-plasma hardening; modified layer; steel; ferrite; perlite; packet and plate martensite*

1. Introduction

Currently, the development of structural and functional materials based on iron is carried out under the conditions of ever-increasing competitive pressure from the rapidly developing production of alloys of light metals, polymers, ceramics, glass, composites, etc. On the other hand, there is a continuous increase in requirements for strength indicators, wear resistance, cold resistance, and other mechanical properties. To meet these requirements adequately and to resist the negative trends, new technological solutions, effective resource-saving technologies for metal processing are needed [1–3]. One of the resource-saving methods of hardening materials is the method of plasma electrolytic processing of materials [4, 5]. This method allows for various types of surface treatment such as carburizing, nitriding, nitrocarburizing, boriding, sulfiding and hardening (surface hardening) and other types of heat treatments [6–10]. Among them, the plasma electrolytic hardening (surface hardening) is of particular interest [10, 11]. However, there is very little information published on the use of plasma electrolytic hardening (PEH) for surface hardening. The surface hardening process has usually been carried out using a laser beam, an electron beam and a plasma beam [12, 13]. Among them, the most preferable in terms of economic efficiency is plasma hardening. PEH compares favorably with plasma hardening by a high cooling rate and a lower degree of

*E-mail: kozhanovars@yandex.kz

© 2020. This is an open access article distributed under the Creative Commons Attribution-NonCommercial-NoDerivatives 4.0 License. (http://creativecommons.org/licenses/by-nc-nd/4.0/)

oxide layer formation. As such, plasma discharges are formed between the metal surface and the electrolyte and the cooling process is carried out in a flowing electrolyte. Earlier, we have developed the method of cathodic PEH, which allows increasing tribological properties of structural steels [14, 15]. Its essence lies in the rapid and short-term concentrated heating of the working surface by plasma exposure and subsequent rapid cooling by heat removal from the depth of the sample by flowing electrolyte in contact with the treated surface [16]. In the literature [14–16] it was shown that after PEH phase, structural transformations occur in the surface layer and the wear resistance and hardness of chromium-nickel steels increase. It is known that the reason for the increase in mechanical properties after plasma hardening is the formation of a finely dispersed martensitic structure [17, 18]. In the literature [19, 20] it is also shown that after plasma hardening of surface layer, martensite with a packet morphology and cementite interlayers are formed along the boundaries of martensite crystals. However, there is practically no data on the fine structure of steels treated by plasma electrolytic surface hardening. Therefore, it is of interest to study structural-phase transformations in steels during PEH. Thus, the elucidation of the physical mechanisms of the formation and evolution of structural-phase states in steels is one of important tasks of modern physics of condensed matter. It is based on the development of effective ways to improve the performance [5, 21]. In this regard, the aim of the study was to determine the phase composition and parameters of the fine structure after PEH and compare them with the initial state of steel.

2. Experimental

In accordance with the tasks set, 0.34C–1Cr–1Ni–1Mo–Fe steel (GOST 8479-70) was chosen as the research object. PEH of steel samples was carried out by surface hardening with rapid concentrated heating of the surface by plasma exposure and subsequent rapid cooling by heat removal from the depth of the sample by electrolyte jet [20]. PEH was conducted at the Research Center "Surface Engineering and Tribology" of S. Amanzholov East Kazakhstan State University on UEPOM-M technological system (Fig. 1). The installation consisted of a chamber for electrolyte-plasma processing of materials, a personal computer and a power supply with capacity of 40 kW [22]. The PEH of steel samples was carried out in a cathodic mode in aqueous solution containing 20 % sodium carbonate and 10 % carbamide. To heat the sample to the hardening temperature, a voltage of 320 V was applied between the electrodes for 2 seconds, then the voltage was turned off and the sample was rapidly cooled due to heat removal from the base and due to the flowing electrolyte. When heated, the current density was 25 A/cm^2 to 30 A/cm^2. In such mode, an intensely glowing plasma layer was formed in the cathode region and the sample was heated at a rate of 450 °C/s to 500 °C/s. Steel samples with the size of 30 mm × 30 mm × 15 mm were treated, while the area of the hardened zone was 12 mm^2 (the hole size of the cone-shaped partition was 10 mm). The PEH process was performed without reflow. Due to the short duration process, the surface roughness practically has not changed after PEH [15, 23].

Microhardness of steel samples was measured in the PMT-3 device in accordance with GOST 9450-76, under the load on the indenter P = 1 N and holding time of 10 seconds. The study of the fine structure and phase composition was carried out by transmission electron microscopy (TEM) on thin foils using EM-125 electron microscope at an accelerating voltage of 125 kV. The working magnification in the microscope column was ×25,000 to ×50,000. The study of the steel samples was carried out in two states: 1 – before PEH (initial state); 2 – after PEH at the surface of the samples. Determination of phases was carried out using images confirmed by microdiffraction patterns and dark-field images obtained in the reflections of the corresponding phases. The images obtained with the electron microscope were used to measure the volume fractions of morphological components of the steel matrix as well as the sizes, distribution density and volume fractions of carbide particles. Determination of linear dimensions was carried out by the secant method according to standard techniques [24]. All data obtained were processed

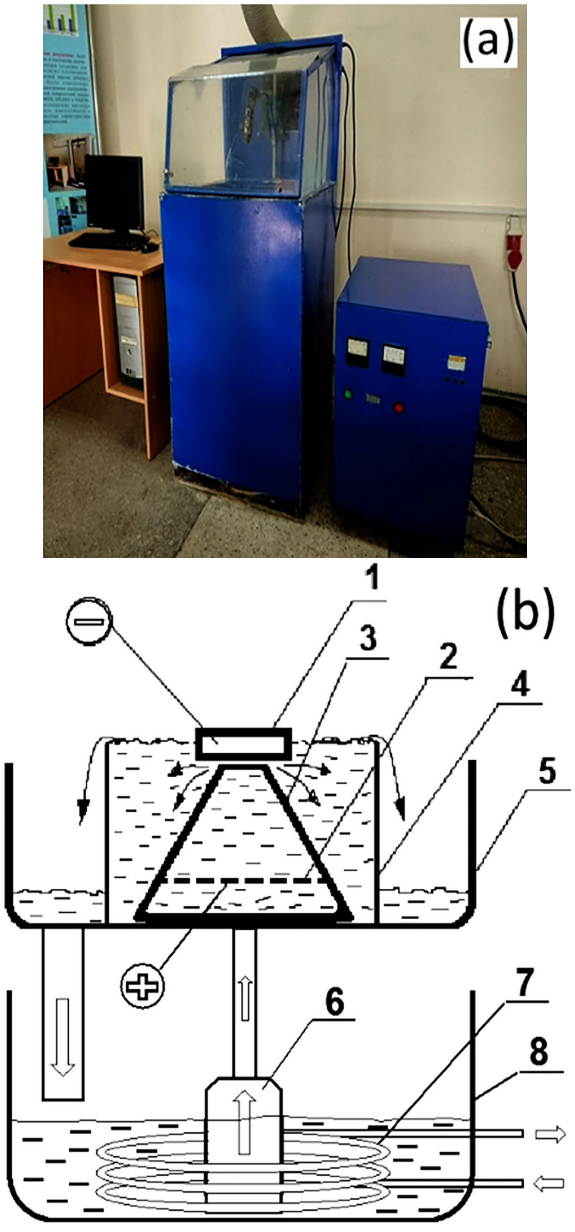


Fig. 1. Photograph (a) and scheme (b) of UEPOM-M EPT system: 1 – processed sample (cathode), 2 – stainless steel anode, 3 – cone-shaped partition, 4 – electrolytic cell, 5 – pallet, 6 – pump, 7 – heat exchanger, 8 – bath with electrolyte.

statistically. The phase composition and parameters of the fine structure after surface hardening were determined and compared with the initial state of the steel (the study of the initial state of the steel was carried out earlier and used as a comparison with the results obtained in this work).

3. Results and discussion

Fig. 2 shows a graph of the change in microhardness through the depth of the 0.34C–1Cr–1Ni–1Mo–Fe steel sample treated by PEH method. A significant increase in microhardness is seen near the surface. The transition zone from the hardened layer to the basement is smooth, while the microhardness of the transition zone is slightly less than that of the basement and the microhardness of the basement does not change. The modified layer thickness is ~1800 mμ. In order to detect structural and phase changes in the surface layer of 0.34 C-1Cr–1Ni–1Mo–Fe steel at PEH TEM studies were performed.

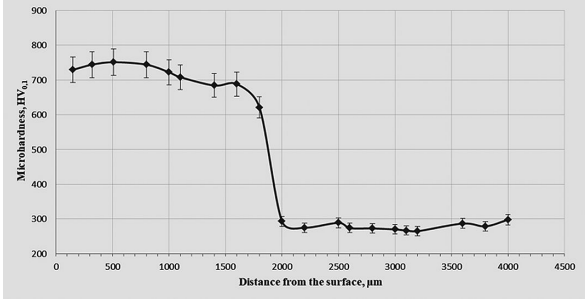


Fig. 2. Graph of microhardness distribution through the depth of 0.34C–1Cr–1Ni–1Mo–Fe steel after PEH.

As shown in earlier studies [25, 26], in the initial state, the structure of 0.34C–1Cr–1Ni–1Mo–Fe steel is: (1) lamellar pearlite, (2) ferrite-carbide mixture, and (3) fragmented ferrite. Lamellar perlite is present in almost perfect and fragmented forms. An electron microscopic image of lamellar pearlite in 0.34C–1Cr–1Ni–1Mo–Fe steel is shown in Fig. 3a. The volume fraction of pearlite in 0.34C–1Cr–1Ni–1Mo–Fe steel in initial state is 35 %, of which the ideal pearlite and fragmented pearlite fraction is 10 % and 25 %, respectively. Thus, our earlier studies have shown that 0.34C–1Cr–1Ni–1Mo–Fe steel in the initial state is a deformed material. The average scalar dislocation density in steel is 2.2×10^{-10} cm^{-2} [26].

The structure of the steel after surface hardening was studied in the near-surface layer of the sample. Surface hardening of 0.34C–1Cr–1Ni–1Mo–Fe steel led to significant qualitative and

quantitative changes in the steel structure, namely, to a change in the phase composition and the types of phases present, as well as their morphology. Thus, both the phase composition and the fine structure of steel in the near-surface layer of the sample differ significantly from the initial state.

The studies have shown that surface hardening led to the formation of a martensitic structure. The morphology of the fine structure is represented by a mixture of packet and lamellar martensite, i.e. packet-lamellar martensite. A typical electron microscopic image of the fine structure of 0.34C–1Cr–1Ni–1Mo–Fe steel after surface hardening is shown in Fig. 3b. The average transverse dimension of an individual strip is 0.25 μm. The volume fraction of packet martensite in the structure of deposited layer in the initial state is 60 %. The transverse size of the plates is substantially larger than the transverse size of an individual flow. The average transverse dimension of an individual plate is 1.1 μm. The volume fraction of lamellar martensite is 40 %.

It has been established that the matrix of the packet-lamellar martensite is the α-phase. As in the initial state, the crystal lattice of the α-phase remains body-centered cubic (BCC), which is a solid solution based on iron atoms, interstitials (C, N, etc.) and substitutions (Cr, Ni, Mo, V, etc.), simultaneously. The main sites in the crystal lattice of the α-phase are occupied, first of all, by iron atoms, as well as by substitutional elements; the interstitial sites (mainly tetrahedral interstices) are partially occupied by carbon atoms.

The indexing of microdiffraction patterns obtained from the fine structure of steel after surface hardening showed that, in addition to reflections of the α-phase, the microdiffraction patterns contain reflections belonging to γ-phase. Such an example is shown in Fig. 3. It means that the γ-phase is the second morphological component of the matrix of the steel under study. The γ-phase is present in the form of retained austenite, formed because of incomplete martensitic transformation during surface hardening of steel.

The study by electron microscopy showed that the residual austenite (γ-phase) in the packet and lamellar martensite is located along the boundaries

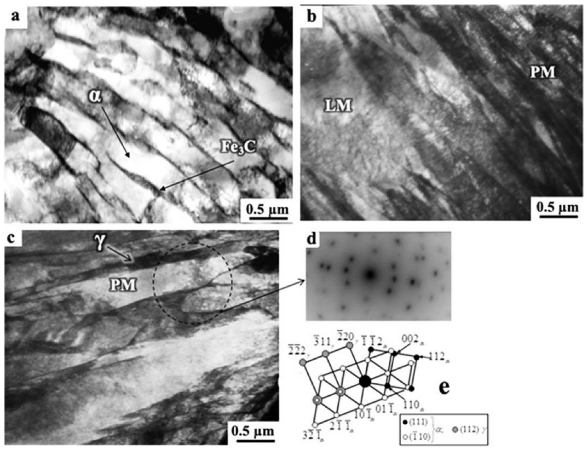


Fig. 3. TEM images of 0.34C–1Cr–1Ni–1Mo–Fe steel before and after surface hardening, (a) initial state, (b), (c) after surface hardening (PM – packet (lath), LM – lamellar martensite), (d) microdiffraction pattern, (e) its indexed diagram (there are reflections related to (1 1 1) and ($\bar{1}$10) planes of α-phases and (1 1 2) of γ-phases).

of martensite crystals in the form of long thin layers (Fig. 4). In addition, it is also located in lamellar martensite, inside the martensite plates and has the form of "needles" (Fig. 4). The crystal lattices of the retained austenite and the α-matrix, regardless of the type and location of the retained austenite, are always related to each other by the Kurdjumov-Sachs orientation relation. This is confirmed by the microdiffraction patterns shown in Fig. 4c and their indexed diagrams.

At the boundaries of the martensite laths, there is residual austenite (γ-phase) in the form of thin interlayers (Fig. 4). The presence of γ-phase is confirmed by the dark-field image (Fig. 4b) represented by the [2$\bar{2}$0] reflection of γ-phase in the microdiffraction pattern obtained from this area (Fig. 4), and its indexed diagram (Fig. 4). As can be seen from the microdiffraction pattern and its indexed diagram, the [$\bar{2}$00] α direction coincides with the [$\bar{2}\bar{2}$0] γ direction (the coinciding directions in Fig. 4 are marked with an arrow). The example shown in Fig. 4a confirms that the crystal lattices of retained austenite, located inside martensite plates in the form of “needles,” and the α-matrix are also interconnected by the Kurdjumov-Sachs orientation relation. The performed calculations

showed that the volume fraction of retained austenite (γ-phase) in packet martensite is 5 %, in lamellar martensite: 7 %, while 6 % of it is contained within the martensite plates. In general, for the material (taking into account the volume fractions of packet and lamellar martensite), the volume fraction of retained austenite is 5.8 %.

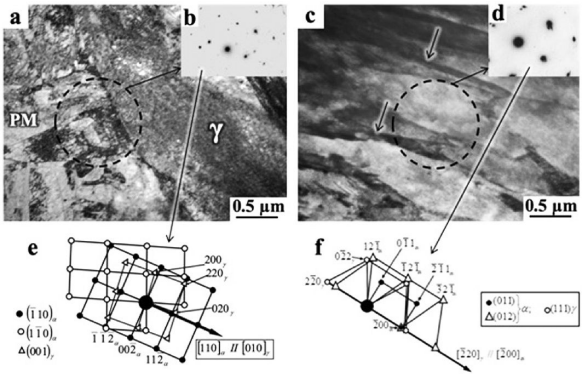


Fig. 4. TEM images of 0.34C–1Cr–1Ni–1Mo–Fe steel after surface hardening, (a) bright field image: packet martensite (P – packet, γ – residual austenite in the form of a colony), (b) microdiffraction pattern obtained from the area marked by the circle; (c) bright field image: isolation of the γ-phase along the boundaries of the batten α-phase laths (arrows indicate the layers of retained austenite (γ-phase) at the boundaries of the martensite laths); (d) microdiffraction pattern obtained from the area marked by the circle; (e), (f) indexed diagrams of microdiffraction patterns.

PEH of 0.34C–1Cr–1Ni–1Mo–Fe steel led to formation of particles of carbide phase in the packet-lamellar martensite, namely, cementite and complex $M_{23}C_6$ carbide. Particles of cementite are present only inside all martensite crystals (in laths and plates). Examples are shown in Fig. 5. As can be seen from the presented figures, in all martensite crystals, cementite particles have a form of thin elongated plates which are located in two and three directions relative to the axis of the martensite crystal. The average particle size in martensite laths is 12 nm $\times$ 32 nm. In martensite plates, cementite particles are larger; their average size is 20 nm $\times$ 80 nm. The volume fraction of cementite in packet (lath) martensite is 0.6 %, in lamellar: 1.5 %, i.e. 2 times more. It is clearly seen in the presented micrographs that the particles are not only larger, but the distribution density of cementite particles in lamellar martensite is higher, i.e. the distance between cementite particles in lamellar martensite (r = 60 nm) is less than in packet (r = 100 nm).

In addition to cementite, as noted above, the steel structure also contains $M_{23}C_6$ carbides. M_6C, $M_{12}C$ and $M_{23}C_6$ carbides have a cubic crystal lattice (space group Fd3m). These carbides include Fe_4Mo_2C, $Fe_6Mo_6C_6$, $Fe_{21}Mo_2C_6$, $Fe_{21}Cr_2C_6$. They stand out inside and along the boundaries of crystals of α-phase (martensite laths and plates). The examples are shown in Fig. 5.

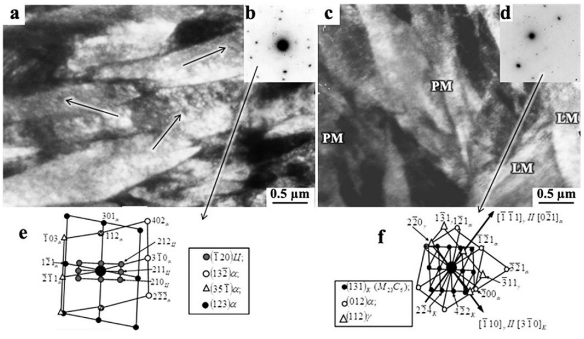


Fig. 5. TEM images of 0.34C–1Cr–1Ni–1Mo–Fe steel after surface hardening, (a) bright-field image: cementite particles inside martensite laths, (b) microdiffraction pattern; (c) bright-field image: $M_{23}C_6$ carbide (marked with the letter K near the indexed reflections) in interlayers of retained austenite located along the boundaries of martensite plates; (d) microdiffraction pattern; (e), (f) indexed diagrams of microdiffraction patterns.

Formation of $M_{23}C_6$ carbides inside the crystals of α-phase is due to the dissolution of cementite which was present in the initial steel and the escape of carbon to the boundaries of α-phase crystals, dislocations and other defects (vacancies, subboundaries, grain boundaries, microcracks) of the crystal lattice of ferrite matrix. $M_{23}C_6$ particles present inside the martensite crystals have a rounded shape and are located on dislocations. It confirms the fact that carbon located on dislocations is spent on the formation of $M_{23}C_6$ carbides. Their average size in packet martensite is 8 nm, the

volume fraction is 0.15 %. In lamellar martensite, the average particle size is 16 nm, the volume fraction is 0.35 %.

Carbides located at the boundaries of α-phase are formed from the γ-phase. It can be proved by the fact that they are observed inside the layers of retained austenite. In addition, the crystal lattices of the γ-phase and these carbides are linked by the "cube-cube" orientation relation. The particles are also rounded. The average size of these particles in both packet and lamellar martensite is not more than 5 nm, however, their distribution density (distance between particles) in the packet and lamellar martensite is different: in packet martensite r = 10 nm, in lamellar: r = 14 nm. The volume fractions of the γ-phase in packet and lamellar martensite are 0.38 % and 0.17 %, respectively. Taking into account these numbers, the volume fraction of $M_{23}C_6$ carbides in the packet martensite, at the boundaries of martensite laths is 0.02 %, in lamellar martensite: 0.002 %.

Thus, it can be argued that the formation of $M_{23}C_6$ carbides is caused, firstly, by the decomposition of martensite (α-phase) and retained austenite (γ-phase), secondly, by the partial dissolution of cementite and, thirdly, by the escape of carbon from dislocations and boundaries of crystals of the α-phase. It means, carbon from α- and γ-solid solutions, cementite particles and crystal lattice defects is consumed for the formation of $M_{23}C_6$ carbides.

As follows from the above figures, the dislocation structure in both packet and lamellar martensite is dense dislocation network. The average scalar dislocation density ρ, calculated by the rectangular grid method, in packet martensite turned out to be 3.78×10^{-10} cm^{-2}. In lamellar martensite, the average value of ρ is lower and amounts to 3.0×10^{-10} cm^{-2}. In general, for the material $\rho = 3.47 \times 10^{-10}$ cm^{-2}.

The dislocation structure in both packet and lamellar martensite is polarized. This is confirmed by the presence of bending extinction contours in all martensite crystals, which are clearly visible on electron microscopic images. Such contours do not result from deformation of the sample during the production of thin foil, since the technique used in the preparation of foils completely excludes the introduction of artifacts. The presence of extinction contours is the result of bending of crystal lattice, or bending of α-matrix crystal. In this case, only a small part of the crystal is in the exact reflective position (contour). The smaller the contour width, the more the crystal is bent. By measuring and calculating the average thickness (the value of the transverse dimension) of the extinction contour in any area of the material it is possible to determine the amplitude of the torsion-curvature of the crystal lattice χ.

The measurements of the width of the extinction contours showed that in the packet martensite, the average width of the contour is smaller than in the lamellar one. This means that the amplitude of the torsion-curvature of the crystal lattice of α-phase in the packet martensite ($\chi = 515$ cm^{-1}) is greater than in the lamellar ($\chi = 460$ cm^{-1}), i.e. the crystal lattice in packet martensite is more curved than in the lamellar one.

It is known that bending-torsion of the crystal lattice can be plastic (then $\chi = \chi_{pl}$) and elastic (then $\chi = \chi_{el}$). In the first case, it is due to charge dislocation, i.e. excess density of dislocations $\rho\pm$, localized in a certain volume of the material, where $\rho\pm = \rho+ - \rho- \neq 0$ ($\rho+$ and $\rho-$ are the density of positively and negatively charged dislocations, respectively). In the second case, unrelaxed elastic strains accumulate due to incompatibility of deformation, for example, grains. Elastic-plastic bending is also possible ($\chi = \chi_{pl} + \chi_{el}$) when both sources of fields are present in the material. To determine the type of bending, the excess dislocation density $\rho\pm$ was calculated according to the formula:

$$\rho\pm = \chi/b \qquad (1)$$

where b is the Burgers vector of the α-iron. In packet martensite, the average $\rho\pm$ value is $\rho\pm = 2.06 \times 10^{-10}$ cm^{-2}, in lamellar: $\rho\pm = 1.84 \times 10^{-10}$ cm^{-2}. For the material, $\rho\pm = 1.97 \times 10^{-10}$ cm^{-2}. Comparing the obtained values of $\rho\pm$ with ρ in each structural component, it can be assessed that both in packet and lamellar martensite, i.e. in the whole material, the condition $\rho > \rho\pm$

Table 1. Calculated quantitative parameters of the fine structure of 0.34C–1Cr–1Ni–1Mo–Fe steel before and after PEH.

	Average quantitative parameters of fine structure					
	P_V	ρ [cm^{-2}]	$\rho_\pm$ [cm^{-2}]	χ [cm^{-1}]	σ_L [MPa]	σ_d [MPa]
After surface hardening						
Packet martensite	60 %	3.78×10^{-10}	2.06×10^{-10}	515	390	285
Lamellar martensite	40 %	3.0×10^{-10}	1.84×10^{-10}	460	345	270
In the material	100 %	3.47×10^{-10}	1.97×10^{-10}	495	370	280
Initial state						
In the material	100 %	2.20×10^{-10}	~0	~0	295	~0

is fulfilled. This means that the amplitude of the torsion-curvature of the crystal lattice in the entire material: $\chi = \chi_{pl}$, and the bending-torsion of the crystal lattice is of a plastic nature and is caused only by charge dislocation, i.e. excess density of dislocations. The amplitude of the moment internal strains was calculated. It turned out that in the packet martensite $\sigma_d = 285$ MPa, in the lamellar: 270 MPa. In general, for the material $\sigma_d = 280$ MPa. It is known [27] that, when dislocations in a material result in a defective structure, there is another type of internal strains: shear strain σ_L (strain created by the dislocation structure). The calculations showed that $\sigma_L = 390$ MPa in packet martensite, 345 MPa in lamellar martensite, and 370 MPa in the whole material.

The calculated quantitative parameters of the fine structure of 0.34C–1Cr–1Ni–1Mo–Fe steel after surface hardening for each morphological component (in packet and lamellar martensite) as well as for the material as a whole, are presented in Table 1. For comparison, the same table shows the material averaged quantitative parameters of the fine structure of the initial state of steel.

Apparently, from Table 1, the scalar dislocations density of package and lamellar martensite after surface hardening is higher than in the initial state. After treatment, the excess dislocation density of the package and lamellar martensite is 2.06×10^{-10} cm^{-2} and 1.84×10^{-10} cm^{-2}, and the value of crystal lattice curvature-torsion of the package and lamellar martensite is 515 cm^{-1} and 460 cm^{-1}, respectively. The excess dislocation density and the value of the crystal lattice curvature-torsion of the initial (untreated) material were $\rho_\pm = 0$ and $\chi = 0$. In the whole material after surface hardening, as in the initial state, the following conditions existed $\rho > \rho_\pm$ and $\sigma_L > \sigma_d$. It means that the bending-torsion (distortion) of 0.34C–1Cr–1Ni–1Mo–Fe steel crystal lattice after PEH had also purely plastic character, which did not lead to the formation of microcracks in the material.

4. Conclusions

The studies carried out using the method of transmission electron diffraction microscopy showed that:

- surface hardening of 0.34C–1Cr–1Ni–1Mo–Fe steel of ferrite-pearlite class led to the change in the structural-phase state and the formation of packet-lamellar martensite;
- surface hardening led to the release of fine particles of cementite and $M_{23}C_6$ carbide, evenly distributed throughout the material volume;
- surface hardening led to the polarization of the dislocation structure, distortion of the crystal lattice and formation of internal long-range strains, however, the bending-torsion of the crystal lattice was purely plastic in nature, not leading to the formation of microcracks in the material;
- surface hardening has led to an increase in all quantitative parameters of the fine structure (ρ, $\rho\pm$, χ, σL, σd), which may lead to

additional hardening of the material at the yield point;

- formation of new boundaries (laths and plates) and evenly spaced small particles of the carbide phase (cementite and $M_{23}C_6$) may also lead to significant strengthening of the steel in comparison with the initial state.

Acknowledgements

The paper was performed within the grant financing of scientific research for 2018-2020 of the Committee of Science of the Ministry of Education and Science of the Republic of Kazakhstan. The Grant No. AP05134936.

References

[1] HE K., WANG L., *Renew. Sust. Energ. Rev.,* 70 (2017), 1022.

[2] OGI T., NANDIYANTO A., OKUYAMA K., *Adv. Powder Technol.,* 25 (1) (2014), 3.

[3] KRISHNA L., MADHAVI Y., BABU P.S., SRINIVASA D., PADMANABHAM G., *Mater. Today,* 15 (2019), 145.

[4] PADERVAND S., AMIRI M., MOUSAVI M., *Int. J. Refract. Met. H.*, 87 (2020), 105146.

[5] SKAKOV M., RAKHADILOV B., SCHEFFLER M., BATYRBEKOV E., *Mater. Test.,* 57 (4) (2015), 360.

[6] DYAKOV I., BUROV S., BELKIN P., ROZANOV E., ZHUKO S., *Surf. Coat. Tech.*, 362 (2019), 124.

[7] PEZZATO L., BRUNELLI K., DOLCET P., DABALÀ M., *Surf. Coat. Tech. A,* 307 (2016), 73.

[8] WANG B., JIN X., XUE W., WU ZH., DU J., WU J., *Surf. Coat. Tech.*, 232 (2013), 142.

[9] KUSMANOV S., GRISHINA E., BELKIN P., KUSMANOVA Y., KUDRYAKOVA N., *Met. Sci. Heat. Treat.,* 59 (1) (2017), 117.

[10] BELKIN P., KUSMANOV S., *Surf. Eng. Appl. El.,* 52 (6) (2016), 531.

[11] BELKIN P., KUSMANOV S., SMIRNOV A., *Mater. Sci. Forum,* 844 (2016), 146.

[12] ZHANG H., SHI Y., CY X., KUTSUNA M., *Surf. Eng.,* 19 (2) (2003), 134.

[13] YULEI F., JING H., SHEN X., WANG Y., ZHAO W., *Nucl. Instrum. Meth. B,* 410 (2017), 207.

[14] RAKHADILOV B., ZHUREROVA L., PAVLOV A., *IOP Conf. Ser. Mater. Sci. Eng.,* 142 (2016), 1.

[15] RAKHADILOV B., BURANICH V., SATBAYEVA Z., SAGDOLDINA Z., KOZHANOVA R., POGREBNJAK A., *J. Mater. Res. Technol.*, 9 (4) (2020), 6969.

[16] SATBAEVA Z., BAYATANOVA L., KILYSHKANOV M., KALIBAYEV K., KOCHNEVA A., *J. Phys. Conf. Ser.,* (2019), 231.

[17] BESPALOVA A., LEBEDEV V., FROLENKOVA O,, KNYSH A., DASHKOVSKAYA O., FAYZULINA O., *EEJET*, 4/12 (100) (2019), 52.

[18] XIANG Y., YU D., CAO X., LIU Y., YAO J., *P. I. Mech. Eng. J.-J. Eng.,* 232 (7) (2017), 787.

[19] EFIMOV O., IVANOV Y., GROMOV V., YUR'EV A., PISKALENKO V., *Steel Transl.,* 42 (2012), 489.

[20] BELOV E., EFIMOV O., YUR'EV A., IVANOV Y., GROMOV V., *Steel Transl.,* 41 (2011), 102.

[21] SUMINOV I., BELKIN P.I.D.R., *Tekhnosfera*, 1 (2011), 464 [in Russian].

[22] RAKHADILOV B.K., SAGDOLDINA Z.B., SATBAEVA Z.A., *Patent for utility model of the Republic of Kazakhstan*, 5354 (2020), 25.

[23] RAKHADILOV B.K., SATBAEVA Z.A., BAYATANOVA L.B., KILYSHKANOV M.K., KALIBAYEV K.A., KOCHNEVA A.K., *J. Phys. Conf. Ser.*, 1393 (2019), 012119.

[24] HIRSCH P.B, *R. E. Krieger Publishing Company*, 1977, p. 563.

[25] POPOVA N., ERYGINA L., NIKONENKO E., SKAKOV M., KONEVA N., KOZLOV E., *Bull. Russ. Acad. Sci.: Phys.,* 81 (3) (2017), 354.

[26] POPOVA N., NIKONENKO E., NIKONENKO A., GROMOV V., PEREGUDOV O., *Steel Transl.,* 10 (49) (2019), 671.

[27] KONEVA N., TRISHKINA L., KOZLOV E., *Fundamentalnyye Problemy Sovremennogo Materialovedeniya,* 11 (1) (2014), 40 [in Russian].

Received 2020-08-29
Accepted 2020-11-17